IEEE Access
Multidisciplinary ⋮ Rapid Review ⋮ Open Access Journal

Received 8 May 2024, accepted 25 June 2024, date of publication 1 July 2024, date of current version 9 July 2024.

*Digital Object Identifier 10.1109/ACCESS.2024.3421368*

RESEARCH ARTICLE

# Advancing Radial Arterial Pulsation Simulation: Wave Decomposition Modeling With Hardware Implementation

**TAE-HEON YANG[1], JAE-IK KIM[2], JEONG-HOI KOO[3], GWANGHYUN JO[4], AND YOUNG-MIN KIM[5]**

[1]Department of Mechanical Engineering, Konkuk University, Seoul 05029, Republic of Korea
[2]Department of Electronic Engineering, Korea National University of Transportation, Chungju-si, Chungbuk 27469, Republic of Korea
[3]Department of Mechanical and Manufacturing Engineering, Miami University, Oxford, OH 45056, USA
[4]Department of Mathematical Data Science, Hanyang University, ERICA Campus, Ansan-si 15588, Republic of Korea
[5]Digital Health Research Division, Korea Institute of Oriental Medicine, Daejeon 34054, Republic of Korea

Corresponding authors: Gwanghyun Jo (gwanghyun@hanyang.ac.kr) and Young-Min Kim (irobo77@kiom.re.kr)

This work was supported in part by Korea Institute of Oriental Medicine (KIOM) under Grant KSN1824130 and Grant KSN1823130, and in part by the Ministry of Food and Drug Safety under Grant 21174MFDS225.

**ABSTRACT** Radial arterial pulse waveforms (RAPWs) have been actively studied for decades as they provide important information on cardiovascular disease risk factors. The primary goal of this study is to propose a new method that accurately simulates and physically implements the realistic pulse wave of the radial artery, taking into account the reflected wave of the fluidic pressure generated by the elasticity of the arterial walls and branching of blood vessels. To this end, this study utilizes the wave decomposition modeling approach, which entails separating a single pulse pressure waveform (PPW) into three waveform components, consisting of one forward wave and two backward or reflective waves. based on the physiology of pulse waveforms. It employs a six-degree-of-freedom mathematical model that integrates the three, and the control parameters of these components can be adjusted to generate the desired pulse waveforms This model is then realized in a physical pulse simulation system using three cylindrical cams with continuously varying surface profiles, each representing forward and backward wave components. By controlling the position, the phase, as well as spin speed and direction of the cams, the simulator can reconstruct desired radial pulse waveforms. To evaluate the performance of the simulator, the reproduced pulse waveforms were compared with approximate radial pulse pressure waveforms based on in vivo data in terms of the augmentation index (AI) and L2 error. The results showed that the errors were less than 5.3 % for all age groups, indicating that the proposed pulse simulator can reproduce the age-specific pulse waveforms corresponding to human radial pulse waveforms. Furthermore, the results demonstrated the consistent and repeatable ability of the pulse simulator to replicate desired pulses, indicating its potential for effective use in palpation training for RAPWs.

**INDEX TERMS** Age-dependent, hemodynamics, radial artery pulse waveform, wave decomposition.

## I. INTRODUCTION

Accurate sensing, measurement, and simulation of radial arterial pulsation is important in the field of medicine, particularly for the evaluation and assessment of cardiovascular health [1], [2], [3], [4], [5]. The pulsation of the radial artery mirrors the cardiac cycle and can provide important information about a person's cardiac function. Radial pulses can be used to develop and improve medical devices such as pulse oximeters and blood pressure monitors. By simulating radial arterial pulsation, researchers and medical professionals can gain a deeper understanding of how various factors, such

The associate editor coordinating the review of this manuscript and approving it for publication was Gyorgy Eigner.

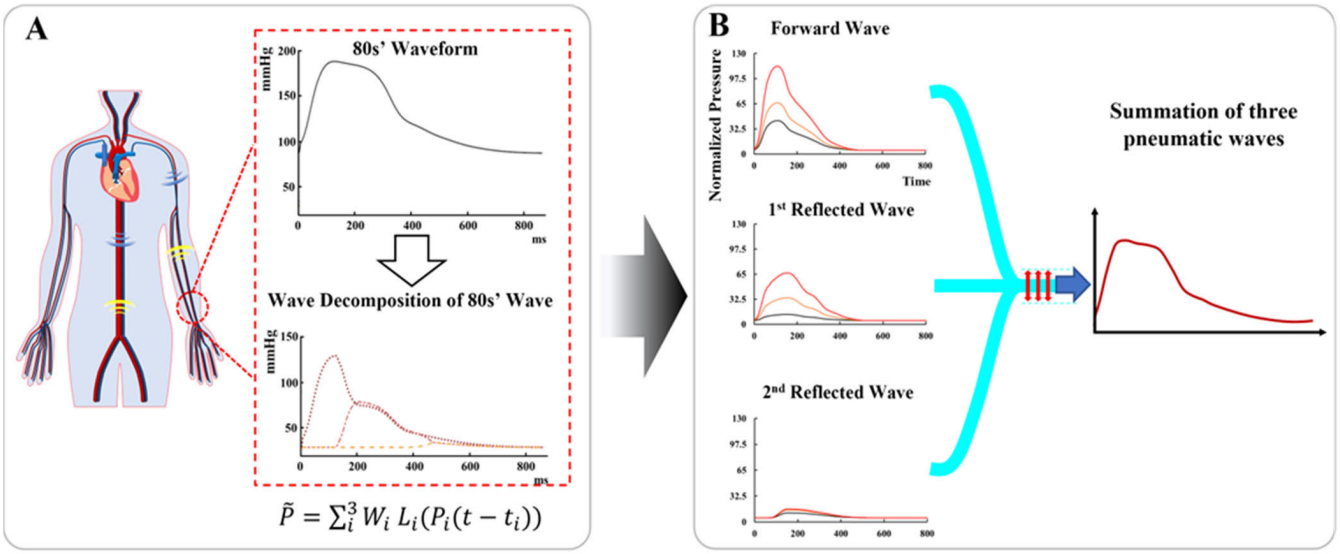


**FIGURE 1.** **Waveform decomposition and reconstruction of blood pulse wave: (a) wave decomposition of 80's pulse pressure based on mathematical model, (b) age-specific waveform reconstruction by summing the forward wave, first reflection wave, and second reflection wave.**

as age, disease, and medications, affect pulsation patterns and blood flow within the radial artery [3]. In addition, simulating radial arterial pulsation can serve as a valuable tool for training healthcare professionals in pulse palpation and measurement techniques. Additionally, it plays a pivotal role in advancing the development of innovative diagnostic tools and methodologies aimed at early detection of cardiovascular diseases and conditions such as hypertension, peripheral artery disease, and coronary artery disease. When developing a simulator for radial artery pulsation, accurately reproducing the blood (fluidic) pressure waveform within the radial artery. This accuracy directly affects the simulation's precision. Failure to adequately capture the dynamics of the pulse wave may compromise the accuracy of the simulator's results, potentially resulting in significant consequences for medical diagnoses and device development.

Understanding the physiology of the circulatory system highlights both the importance and challenges of accurately simulating radial pulses. In particular, the phenomena of reflective waves of fluidic (blood) pressure in the cardiovascular system are crucial, playing a pivotal role in regulating blood flow and maintaining proper blood pressure throughout the body. When the heart contracts, it generates a pulse wave that travels through the arteries, delivering oxygenated blood to the various organs and tissues. However, as this pulse wave travels the arterial system, it encounters resistance from the blood vessels. This resistance leads to the pulse wave being reflected back toward the heart as a secondary wave, known as a reflective wave. Reflective waves play a significantly role in regulating blood flow by reaching the heart during diastole, the relaxation phase of the cardiac cycle. This results in a sudden increase in blood pressure, facilitating blood refilling in the heart and increasing cardiac output. Moreover, the reflective waves help prevent excessive pressure buildup in the arteries by dissipating some of the pulse wave energy as it is reflected back to the heart. However, in certain disease states such as hypertension, atherosclerosis, and heart failure, the reflective wave can become dysfunctional, contributing to a further increase in blood pressure and a decrease in cardiac function. Understanding the importance of reflective waves in cardiovascular physiology enables physicians more effectively diagnose and treat these conditions, ultimately improving patient outcomes.

Recognizing the importance of extracting reflected waves in blood pulsation, numerous studies have explored various methods to decompose the reflected and forward waves within the radial artery pressure waveform (RAPWs). These approaches include Gaussian-type basis functions, which offer an intuitive representation of forward and reflected waveforms, selected through the minimization of an objective function comparing decomposed waveforms to target RAPWs [6], [7], [8]. However, locating the peak of the reflected wave in elderly individuals' waveforms remains challenging. Alternatively, some researchers have employed black-box-type signal-processing methods to decompose RAPWs, for example, independent component analysis (ICA) [9], [10]. Yet, the need for careful parameter section poses challenges in applying ICA to the decomposition of pulse pressure (PP). In contrast to the theses methods, which did not take into account the physiological properties of the cardiovascular system, wave intensity analysis was studied as an approach for decomposing pressure and velocity waveforms, incorporating essential physiological parameters such as characteristic impedances or vessel elasticities [11], [12], [13], [14]. However, the wave intensity analysis presents a challenge in terms of requiring blood velocity measurements in the aortic vessels. Another well-established model for decomposing RAPWs is the wave reflection model,

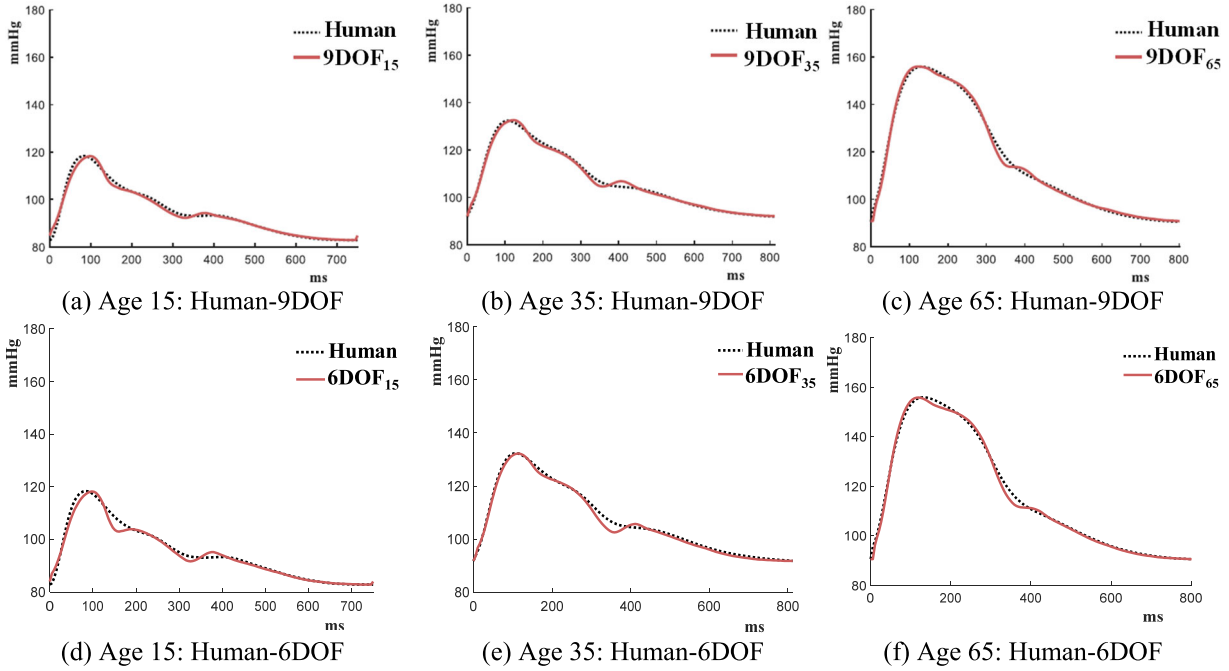


**FIGURE 2. Comparison of waveforms generated by 'Human vs 9-DOF' and 'Human vs 6-DOF' pulse pressure models by ages: (a) comparison of human-9DOF at 15 years old, (b) comparison of human-9DOF at 35 years old, (c) comparison of human-9DOF at 65 years old, (d) comparison of human-6DOF at 15 years old, (e) comparison of human-6DOF at 35 years old, (f) comparison of human-6DOF at 65 years' old.**

which analyzes waveforms by considering the relationships between pulse pressure and flow rate through characteristic impedance [15], [16], [17], [18], [19], [20]. The advantage of wave reflection models lies in their ability to reconstruct flow rate waveforms for both forward and reflected waves by matching the hemodynamic characteristics. Notably, a recent development by one of the authors introduces a method that decomposes waveforms into one forward and two reflected components [20].

The replication of blood (fluidic) pressure and the incorporation of reflective waves into the radial artery pulse waveform typically entail creating a fluidic circuit that emulates the characteristics and dynamics of the human cardiovascular system. Various methods are employed to replicate the radial artery pulse waveform. Pneumatic systems use air pressure, hydraulic systems use fluid pressure, and electromechanical systems use electrical signals to control mechanical actuators for waveform simulation. Electromechanical systems offer greater flexibility and accuracy due to precise control over electrical signals [21], [22], [23]. Additionally, computer models of the cardiovascular system use mathematical equations to simulate the pulse waveform, enabling precise control for research and device development.

When developing hardware or pulse simulators to replicate the radial artery pulse waveform, several approaches are available. Pneumatic systems use air pressure generated by an air compressor to create the required pulse pressure, which is then mimicked using a pneumatic actuator. In contrast, hydraulic systems generate fluid pressure through a pump and employ a hydraulic actuator to replicate the pulse waveform [24], [25], [26], [27], [28], [29], [30], [31], [32]. Moreover, a hybrid system that combines both pneumatic and hydraulic (fluidic) systems can provide a realistic simulation of the human cardiovascular system, leveraging the advantages of both pneumatic and fluidic systems. Nonetheless, the use of these "fluidic" systems in clinical evaluation or training systems is limited due to significant challenges related to accuracy and reproducibility. These challenges primarily result from the inability to maintain consistent flow control. In other words, the behavior of the air or fluid used to generate pulse waveforms can vary depending on working conditions or operational circumstances.

Alterative to existing approaches, this study presents a novel method that offers a reliable means of replicating pulse waveforms, while preserving the fluidic pulse pressure dynamics. It achieves this by utilizing a three-dimensional (3D) cam-follower mechanism, eliminating the use of a working fluid in the system. The 3-D cam is designed based on computational forward and backward (reflective) waves of human arterial fluidic pressures. This method offers several notable benefits. Firstly, it allows for the generation of a wide range of radial artery pulse waveforms, enabling for versatility in simulating different physiological conditions. Secondly, it ensures consistent and reliable replication of pulse waveforms, thereby enhancing the accuracy and reproducibility of simulations. Lastly, the method features a simple control

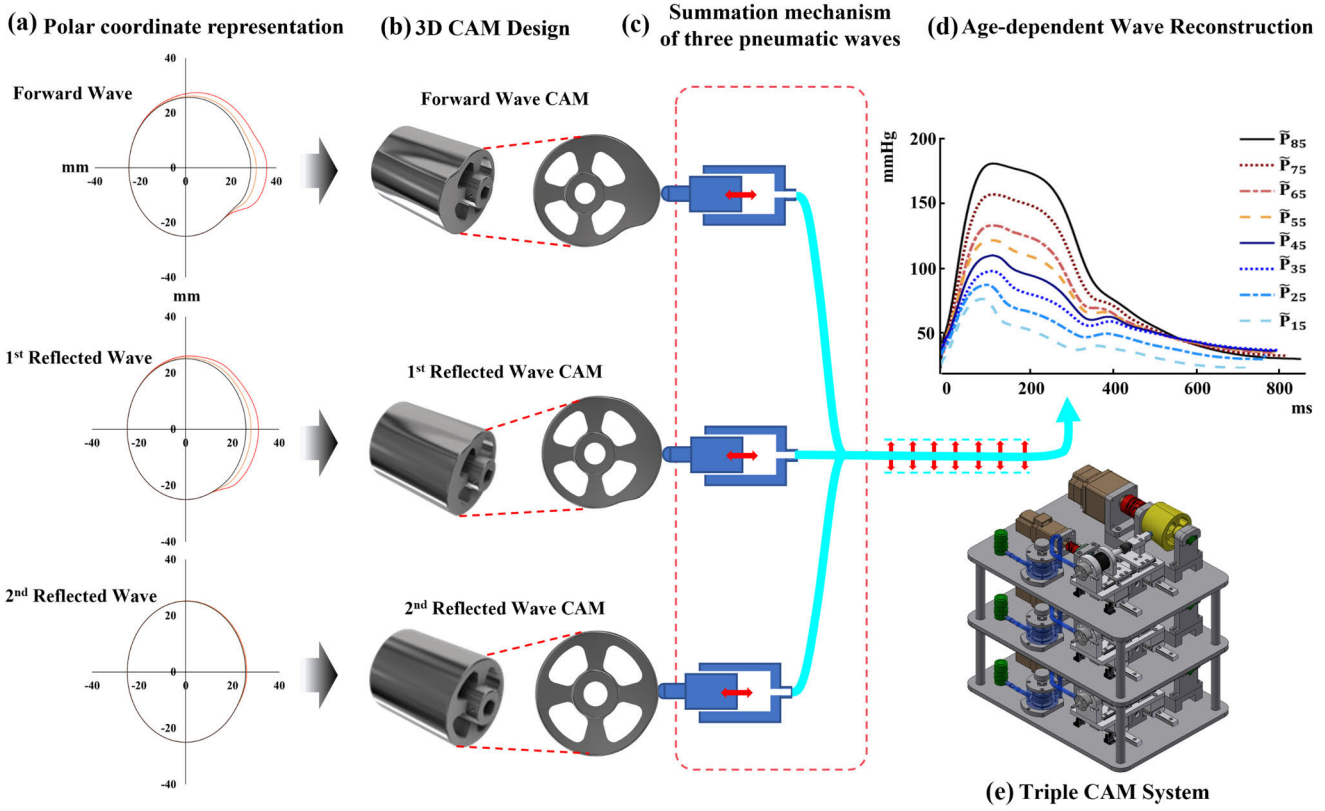


**FIGURE 3.** The conceptual design of triple CAM system based on decomposed waves of Pulses: (a) Polar coordinate representation of pulse pressure waveforms, (b) 3D CAM design for forward wave, 1st reflected wave and 2nd reflected wave, (c) summation mechanism of three pneumatic pressure waves based on cam-follower mechanism, (d) age-specific waveform reconstruction, (e) conceptual design of implemented triple 3D Cam system.

mechanism, making it user-friendly and reducing the complexity associated with generating desired pulse waveforms. In fact, by linearly modulating only two control parameters, namely the pulse magnitude and the pulse arrival time difference (or shifted time, induced by the wave decomposition model of [20]), the cam system can reproduce a desired pulse waveform. The values of the control parameters can be easily determined from the relative translational and angular positions within the 3D cams.

The subsequent section provides an overview of age-specific waveform modulation via triple waveform synthesis and detail the conceptual design based on three 3D cam-follower modules. Next section presents fabrication of the proposed triple cam system. And then, the following section presents experimental results that verify the accuracy and consistency of the proposed method.

## II. WAVE DECOMPOSITION MODELING AND CONCEPTS OF TRIPLE CAM SYSTEM

Figure 1(a) illustrates the blood circulation in the human body. When the heart pumps blood, it generates a forward incidental wave, followed by a first reflected wave is created at the bifurcation of the abdominal aorta and a second reflected wave when it is reflected from a heart valve. Blood carrying this complex pulse pressure waveform then travels through the brachial artery and emits a pulse pressure waveform that can be easily measured using tonometry on the radial artery of the wrist. Subsequently, the blood flows through capillaries before recirculating through the veins. To illustrate the process, Figure 1(a) displays the RAPW of an 80-year-old group alongside its decomposition into a forward wave and two reflected waves. In Figure 1(b), the reconstruction of a pulse waveform is depicted using these three decomposed waves, consisting of one forward wave and two reflected waves.

To investigate whether the complex phenomenon of blood flow can be represented as combinations of multiple waveforms, the authors proposed a mathematical model. Using this model, they demonstrated the regeneration of age-dependent RAPWs by decomposing a single pulse pressure waveform into three waveforms and recreating desired pulses. While additional details can be found in reference [20], the mathematical model is included in equation (1). In this model, $\tilde{P}(t)$ can be utilized to recreate radial pulse pressure waveforms for different age groups by adjusting the control parameters.

$$\tilde{P}_{9-DOF}(t) = \sum_{i=1,2,3} w_i L_{k_i} \{P_i(t - t_i)\} \tag{1}$$

Here, $w_i$ is the weighting parameter, $L_{k_i}$ is the pulse-broadening operator, and $t_i$ is the phase-delay parameter.

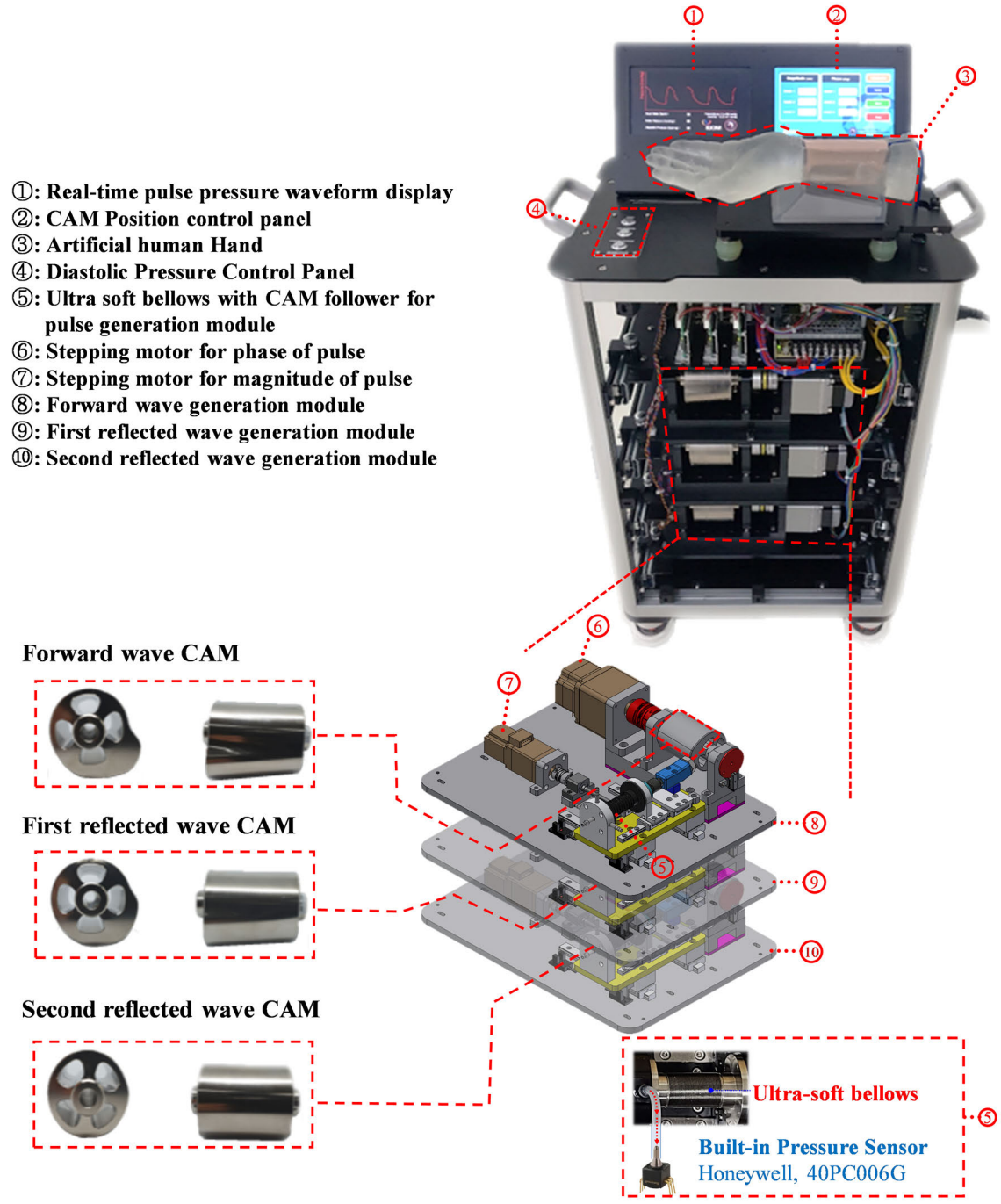


**FIGURE 4.** System configuration of a developed triple 3D-cam based pulse pressure waveform simulator including forward wave 3D-CAM, first reflected wave 3D-CAM and second reflected wave 3D-CAM.

Let us discuss the selection of basis functions $P_i$'s (i=1,2,3). These basis functions corresponds to the forward waveform, the first backward waveform, and the second backward waveform obtained by decomposing waveform of the 85-year-old age group. The decomposition algorithms used in [20] required only three basis functions. In contrast, other choices of basis functions, such as radial-type basis functions like Gaussian functions, require more than three basis functions. It is noteworthy that, taking the advantage of a simulation study, the mathematical model in [20] used nine degrees of freedom(9-DOF), including $w_i$, $L_{k_i}$ and $t_i$ parameters of each of the three waveforms. However, it is quite challenging to implement $L_{k_i}$ which is a pulse-broadening operator in a physical system. To realize the pulse-broadening operator physically, the width of the waveform must be adjusted within a short pulse period ($\sim$ 700 ms) using a mechanical actuator

or a motor. This study, therefore, intends to modify the 9-DOF model into a 6- DOF reduced model, eliminating $L_{k_i}$ as shown in equation (2).

$$\tilde{P}_{6-DOF}\,(\mathrm{t}) = \sum_{i=1,2,3} w_i \{P_i(t - t_i)\} \tag{2}$$

To evaluate the accuracy of reproducing pulse pressure waveforms in equation (2), following two criteria were considered. First, the Augmented Index (AI) shown in equation (3), a clinically important measure in the cardiovascular system, must match well with the target waveform. Second, the phase differences between the first, second, and third peaks of the reproduced waveform, which is also clinically significant and related to the speed of the aortic reflected wave, must align well with those of the target waveform (human). In equation (2), the Augmented Index can be adjusted efficiently by modifying the $w_i$ index, and the phase difference can be efficiently changed by adjusting the $t_i$ index.

$$\mathrm{AI} = \frac{\text{Late systolic Pulse Pressure}}{\text{Early Systolic Pulse Pressure}} \times 100\,(\%) \tag{3}$$

The role of $t_i$ is to control the interval between peaks of $P_i(t-t_i)$, i = 1, 2, 3. For example, if given a fixed $t_1$ is fixed and, as $t_2$ increases, the reconstructed waveform will exhibit a greater delay of the second peak. Additionally, since $w_i$ represents the weight of the basic function $P_i(t - t_i)$, the Augmentarion Index can be easily adjusted by modifying $w_2$. Consequently, the reduced 6-DOF model can be efficiently reconstructed to match the inter-peak intervals and AI of the target waveform. The optimization problem to approximate Equation (2) to human pulse pressure P for each age is defined as equation (4). The optimization problem is defined as aims to find $w_i$ and $t_i$ that minimize the difference between the target function and the reconstructed function.

$$Find\ \left(\mathrm{w}_\mathrm{i}^*, t_i^*\right) = \mathrm{argmin}_{(w_i,t_i)} \sqrt{\int_T \left(\tilde{P}_{6-DOF} - P_{age}\right) \mathrm{d}s} \tag{4}$$

Using the above optimization function, the performance of the 6-DOF model and the original 9-DOF model were compared by overlying pulse waveforms at human pulses to ensure the efficiency of the reduced 6-DOF model. Figure 2 shows the comparison results for three selective age groups, ranging from younger ages (15-year-old) to older ages (65-year-old). Figure 2(a), 2(b) and 2(c) show graphical comparison between human and 9-DOF pulse wave forms. Otherwise, Figure 2(d), 2(e) and 2(f) show graphical comparison between human and 6-DOF pulse wave forms. It was confirmed that the 6-DOF reduced model represents important characteristics of the pulse waveform as well as the 9-DOF model.

To further analyze the performance quantitatively, errors between 9-DOF and human pulse and errors between the reduced model 6-DOF and human pulse were analyzed, respectively. In this analysis, the $L^2$ error, which represents the discrepancy between consecutive data points through least-squares fitting of the pulse pressure waveforms, was calculated. Additionally, the error in the clinically significant radial augmentation index (AI) or the AI error was examined.

Here, the $L^2$ error, which represents the discrepancy between consecutive data points through least-squares fitting of the pulse pressure waveforms, was calculated. Additionally, we considered the ratio of early to late systolic pulse pressure, which is often referred to as the Augmentation Index (AI) as described in equation(3). Both models can capture two key aspects: 1) the temporal delay between first and second peak, and 2) the ratio of early systolic pulse pressure to late systolic pulse pressure (AI index). However, in terms of absolute differences, the error of the 6-DOF model is higher. This discrepancy arises from the elimination of the pulse-broadening operator $L_{k_i}$ from the reduced 6-DOF model. In a CAM system, waveforms can be easily reconstructed by adjusting the phase and magnitude ($w_i$, $t_i$) of the CAM. However, disregarding the $L_{k_i}$ operator results in increased absolute errors. This reflects the trade-off between control efficiency and accuracy. The results of this comparison are presented in Table 1. As shown in the table, although the error increased, both the $L^2$ error and AI error, when analyzed by age, were found to be less than 10%. This confirms that the 6-DOF reduced model remains within the cumulative tolerance of the entire mechanoelectrical system.

**TABLE 1. Errors of pulse pressure waveforms between human and 9-DOF / 6-DOF models for ages 15, 35, and 65 years.**

| | Human vs 9-DOF | | Human vs 6-DOF | |
|---|---|---|---|---|
| Age | $L^2$ Error | AI Error | $L^2$ Error | AI Error |
| 15 | 5.88 % | 5.97 % | 9.52 % | 7.04 % |
| 35 | 4.56 % | 0.45 % | 7.56 % | 1.94 % |
| 65 | 3.43 % | 1.53 % | 8.27 % | 1.90 % |

## III. DESIGN AND FABRICATION OF THE PROPOSED TRIPLE CAM SYSTEM

After validating the efficacy of the wave decomposition model, this study aims to develop a pulse simulator capable of consistently and repeatedly reproducing age-dependent pulse waveforms. This will be achieved using a simple simulator design based on practical pneumatic actuation. An overview of the proposed simulator, referred to as the 'Triple CAM System', is provided in Figure 3, which is based on a three-dimensional (3-D) cam-follower mechanism. From the mathematical model, three base waveforms are derived, consisting of one forward wave and two reflective waves, represented in the rectangular coordinate system (pulse magnitude vs. time). These waveforms are then converted into the polar coordinate system, as shown in Figure 3(a). The curves in the polar coordinate system represent forward, 1st reflected, and 2nd reflected waves for a range of age-dependent pulse waveforms. To simultaneously and physically represent these

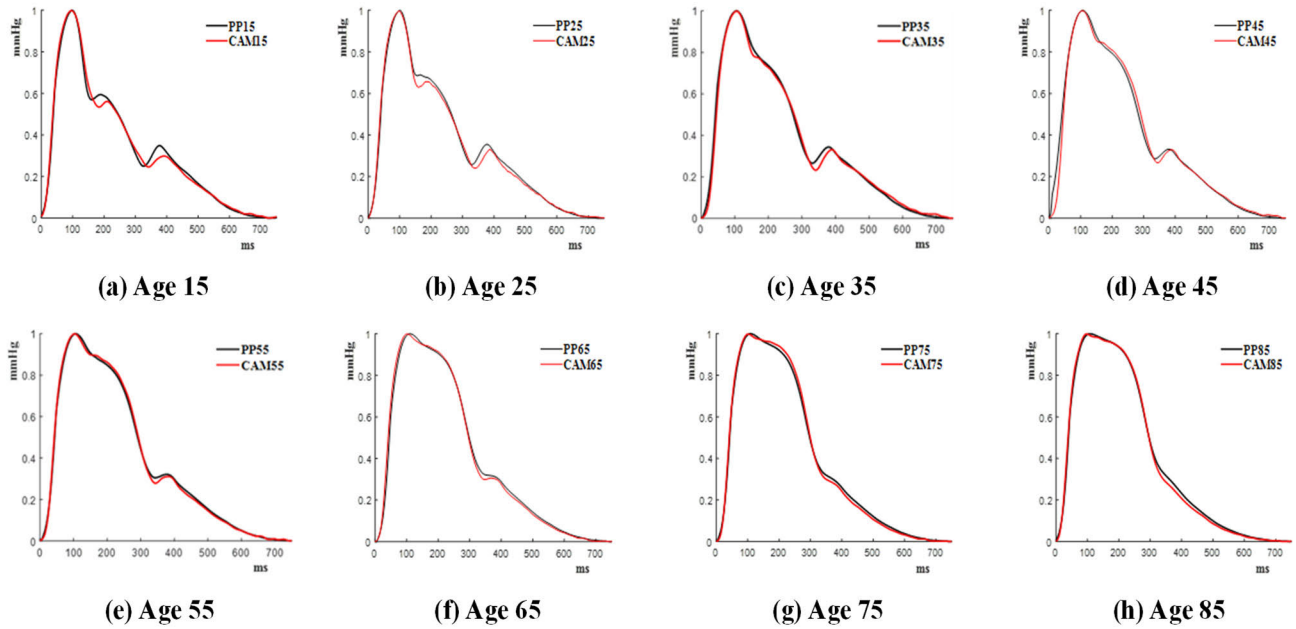


**FIGURE 5.** Comparison of the reproduced pulse pressure waveforms generated by triple-cam system (red) with the human pulse pressure waveforms (black) at ages 15, 25, 35, 45, 55, 65, 75, and 85 years.

waveforms, 3-Dimensional (3-D) cams were constructed so that the contour of each cam represents a continuous variation of the magnitude of pulse waves. In other words, the cam has a continuously varying circular profile, and a cross-section of the cam at a point along its longitudinal direction represents a pulse wave.

More specifically, the shape of the 3D cam depicted in Figure 3(b) is determined based on the 6-DOF model provided in equation (2). For instance, in the case of forward waves, the peak points of the time series at 15, 35, 65, and 85, obtained from equation (2) and presented in Figure 3(a), were connected using least square fitting to define the shape of the 3D cam for forward waves [33]. Similarly, the 3D cams for the first and second reflectors were also designed using the same methodology, respectively.

Stacked in three layers, the rotational and translational motions of 3-D cams can be controlled individually, allowing the reconstruction of a desired pulse waveform. Further details of cam design and fabrication can be found in reference [33].

Figure 4 shows a constructed prototype of the triple cam system along with its components. To generate a pulse pressure wave, the diastolic blood pressure level was first adjusted using the diastolic blood pressure control panel (marked as ④ in Figure 4). The CAM position control panel (labeled as ④ in Figure 4) can then be used to set the initial positions for a desired age group's pulse waveform by adjusting the magnitude and phase delay of the CAMs responsible for the forward, the first reflected, and the second reflected waves. Each pneumatically operated pulse pressure waveform generation module (⑧, ⑨, ⑩ in Figure 4) consists of (1) a 3D CAM designed to mimic the shapes of the forward, first reflected, and second reflected waves, (2) a high-speed stepper motor (PKP546N28A2-TS20 (⑥ in Figure 4)) capable of rapidly rotating the CAM and precisely controlling the rotation angle, and (3) a stepper motor (⑦ in Figure 4) that controls the magnitude of the waveform. Once the initial position is configured according to the age group using the control panel, the CAM rotates to align with the phase delay set by the optical encoder at the designated location. Subsequently, the CAM Follower Module (marked as ⑤ in Figure 4) moves along the linear motion guide to set the magnitude of the CAM.

After the positions are set, the modules are activated to generate the pulse pressure waveform. During system operation, each CAM rotates at high speed, causing the CAM Follower, which is connected to the ultrasoft bellows module, to compress and extend the bellows in accordance with the contour of the CAM. This action generates a pulse wave in the form of air pressure. When each pulse pressure waveform generation module produced compressed air, the waveforms, including the forward, first reflected, and second reflected waves, were consolidated into a complete Pulse Pressure Waveform by the Wave Integration Mechanism through a single air tube. The Pulse Pressure Waveform generated by the Wave Integration Mechanism is output as a real-time pulse pressure waveform display (marked as ① in Figure 4) through a small air pressure sensor (Honeywell, 40PC006G, labeled as ⑤ in Figure 4). An artificial human hand (marked as ③ in Figure 4) with embedded an air pressure tube on the wrist is installed in the system to allow users to feel pulse pressure through the wrist of the hand assembly.

## IV. EXPERIMNETAL EVALUATION OF THE TRIPLE CAM SYSTEM

### A. EVALUATION OF REPRODUCED AGE-SPECIFIC PRESSURE WAVEFORM

In this section, the performance of the triple-cam system in reproducing human pulse pressure is described for a wide range of age groups. By adjusting the stepping motors to control the magnitude and phase of the CAMs, a triple-cam-based pulse simulator produced pulse waveforms ranging in age from 15 to 85 years. The phase and magnitude parameters determined in Section II were substituted into the triple-cam system. Once the triple-cam system generated artificial waveforms for each age, the pulse pressure waveforms were measured with a built-in pressure sensor (Figure 4). Then, the measured waveforms were preprocessed using the method of [34] with a reduced Fourier series function of dimension less than 50 to eliminate spurious noise. Figure 5 shows a comparison of the pulse pressure waveforms generated by the triple-cam at age 15-85 (red) with the human pulse pressure waveforms approximated by the 6-DOF model (black). Overall, the reproduced pulse pressure waveforms had similar shapes to the desired human pulse pressure waveforms. For example, the positions of the first and second peaks coincided. In addition, clinically important AI index were considered.

We quantitatively validated the reproduced waveforms in terms of (relative) $L^2$ and AI errors, as shown in Table 2. The $L^2$ errors and AI errors are less than 5.3 % and 4.3 %, respectively. Indeed, in vivo systolic pulse pressure data obtained from tonometric measurements in human subjects had an average standard deviation of 11.7 % [20]. Thus, compared with the variance of the in vivo data, the levels of $L^2$ and AI errors are acceptable. Therefore, we can conclude that the triple-cam system can reproduce human pulse pressure waveforms. It is noticeable that the $L^2$error and AI error for age 85 are below 2.78 % and 0.21 %, respectively However, the errors tended to increase as the age decreased to 15 years. This appears to be because the contrast between the magnitudes of early and systolic pressures tends to be high at an early age. Therefore, the delaying effects at the conjunction of tubes is more pronounced in the younger age group.

**TABLE 2. Age-specific errors between the reproduced pulse pressure waveforms generated by triple-cam system with the human pulse pressure waveforms.**

| Age | $L^2$ Error | AI Error |
|---|---|---|
| 15 | 5.23 % | 3.08 % |
| 25 | 4.42 % | 4.22 % |
| 35 | 5.28 % | 3.53 % |
| 45 | 3.59 % | 4.30 % |
| 55 | 2.35 % | 2.97 % |
| 65 | 3.79 % | 0.72 % |
| 75 | 3.00 % | 2.11 % |
| 85 | 2.78 % | 0.21 % |

### B. REPRODUCTION OF PATIENT'S PRESSURE WAVEFORM USING TRIPLE-CAM SYSTEM

To demonstrate the performance of the triple-cam system to reproduce non-average (abnormal) human pulse-pressure waveforms, we adopted the waveform of the so-called Pulsus bisferiens (see black colored plots in Figure 6(b)), whose main feature is the appearance of two (unusual) peaks separated by a mid-systolic drop [35]. The design of the cam manipulation using the modified 6-DOF model and the resulting reproduced waveforms are presented. To do this, we developed a mathematical model for the waveforms of patients by tuning the parameters $(t_1, t_2, t_3, w_1, w_2, w_3)$ for age 85 in equation (1), so that the desired modified model has the following form as shown in equation (5):

$$\tilde{P}_{patient}\,(\mathrm{t}) = w_1' P_1\left(t - t_1'\right) + w_2' P_2\left(t - t_2'\right) + w_3' P_3\left(t - t_3'\right) \tag{5}$$

To differentiate the parameters of equation (5) from those of equation (2), new parameters $t_i'$ and $w_i'$ were introduced. $t_i'$ represents the time separated by $T_{Delay}$ from the reference value $t_1$. Since the starting value $t_1'$ and the reference value $t_1$ are the same, $t_1' = t_1$. Here, we denote $T_{Delay_1}$ (and $T_{Delay_2}$, respectively) as the delay between the 1st systolic pressure and the 2nd systolic pressure (and the delay between the 1st and the 3rd systolic pressure). Consequently, $t_2'$ and $t_3'$ are defined as $t_2' = t_1 + T_{Delay_1}$ and $t_3' = t_1 + T_{Delay_2}$, respectively (see Fig. 6(a)). In summary, the formulas related to time are as follows.

$$t_1' = t_1$$
$$t_2' \approx t_1 + T_{Delay_1} \quad t_3' \approx t_1 + T_{Delay_2}$$

Now, we still need to determine the parameters $w_1'$, $w_2'$ and $w_3'$. To express each peak magnitude of the separated blood pressure waveform as a ratio to the peak magnitude of the first forward waveform, an index called $AR$(Amplitude Ratio) was introduced. Here, $AR_1$ was defined as $w_2/w_1$, and $AR_2$ was defined as $w_3/w_1$ (see Figure 6(a)). In summary, the formulas related to magnitude are as follows.

$$w_1' = w_1$$
$$w_2' \approx AR_1 w_1 \quad w_3' \approx AR_2 w_1$$

We propose a modified 6-DOF mathematical model to generate the patient waveforms. By combining the approximation for $t_i'$'s and $w_i'$'s based on the $T_{Delay_i}$'s and $AR_i$'s ($i$= 1, 2), we obtain the following approximation model:

$$\tilde{P}_{patient}\,(t) \approx w_1[P_1\,(t - t_1) + AR_1 \cdot P_2(t - \left(t_1 + T_{Delay_1}\right) + AR_2 \cdot P_3\left(t - \left(t_1 + T_{Delay_2}\right)\right] \tag{6}$$

Figure 6(b) (black) shows the waveform of pulse bisferiens. To implement the patient waveform with a simulator based on the proposed 6-DOF mathematical model, the optimization

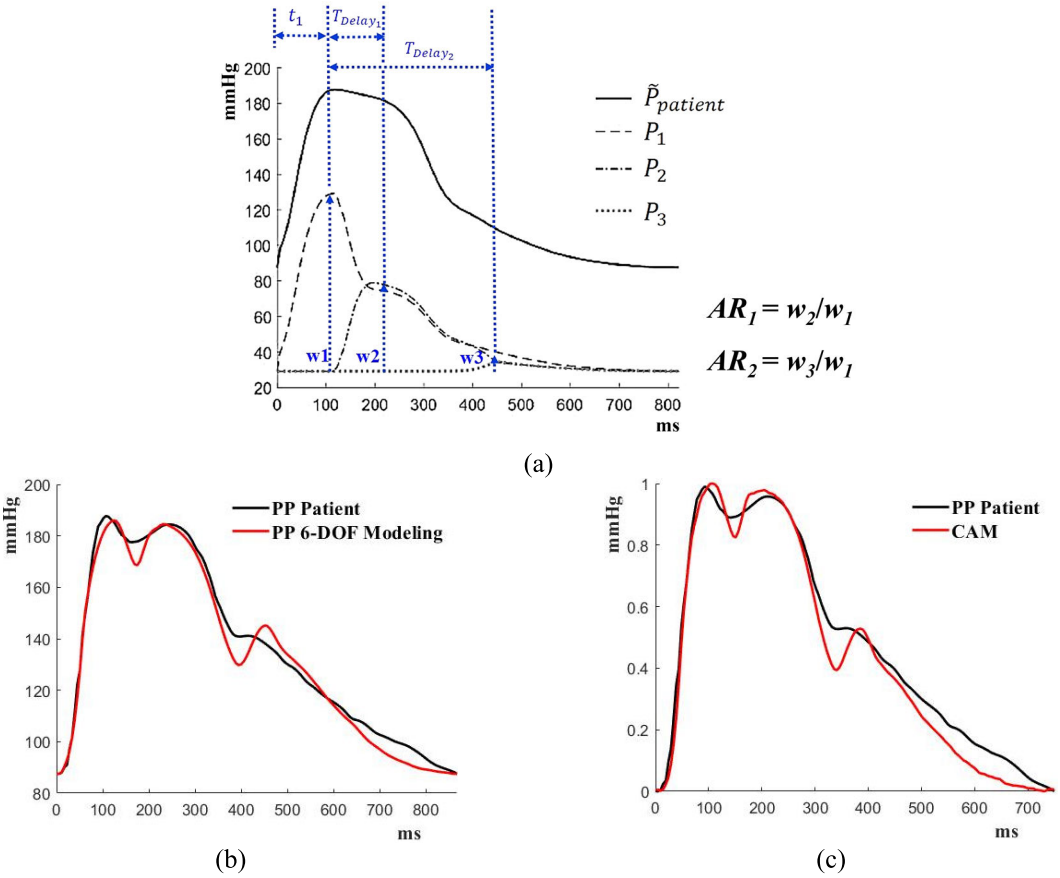


**FIGURE 6.** Parameter setting of wave decomposition in pulse-pressure waveforms and generation of abnormal human pulse-pressure waveforms: (a) Description of the parameters, $T_{Delay_i}$ and $AI_i$ in pulse wave decomposition, (b) Comparison of Pulsus bisferiens waveform (black) and approximated waveform (red) by 6-DOF patient model, (c) Comparison of pulse pressure waveform of Pulsus bisferiens (black) and the pulse pressure waveform generated by the triple-cam system (red).

problem using equation (7) was defined. The optimization problem entails finding $w'_i$ and $t'_i$ that minimize the difference between the target patient function and the reconstructed function.

$$Find\left(w_i'^{*}, t_i'^{*}\right) = \text{argmin}_{(w_i', t_i')} \sqrt{\int_T \left(\tilde{P}_{6-DOF} - P_{patient}\right) ds} \tag{7}$$

Through the optimization analysis, the optimal parameters that can minimize the error between $\tilde{P}_{6-DOF}$ and $P_{patient}$ were determined as follows.

$$T_{Delay_1} = 91.9\,ms, \quad T_{Delay_2} = 280.6\,ms,$$
$$AR_1 = 0.98, \quad AR_2 = 0.59.$$

Substituting the above parameters into (5), an approximate waveform for the patient was obtained. Here, the parameters were slightly adjusted by a post-processing procedure using a line-search algorithm. The resulting approximate waveform for Pulus bisferiens is plotted in Figure 6(b) (red). We see that the 6-DOF based mathematical model can effectively approximate a patient's waveform.

By substituting the magnitude and delay parameters for the stepping motors of the triple-cam system, we obtained a triple-cam-generated waveform for Pulsus bisferiens (see Figure 6(c)). Compared to the target waveform (black), the reproduced waveform (red) is in overall agreement. In particular, the reproduced waveform shows a mid-systolic drop between the two peaks (Figure 6(c), red). In addition, the length of the delay between the 1st and 2nd systolic pressures and the rate of these magnitudes almost match. The $L^2$ errors were 9.43 % and the AI error was 1.17 %. Therefore, the ability of the triple-cam system to reproduce the patient waveforms was verified.

## V. CONCLUSION

This study presents a novel method for accurately mimicking radial artery pulse waveforms with reflected waves of fluidic pressure caused by the elasticity of vascular tubes and the resistance of their branches. By simulating the human cardiovascular system with the proposed device, we observed how

the change in magnitude and phase delay between the forward wave and the corresponding reflected waves affect the risk factors for cardiovascular disease. One of the advantages of the proposed CAM-system is its ability to capture alternations in waveform morphology due to aging or disease. Aging or disease often result in arterial stiffening, leading to a higher AI index in the waveform. In Figure 2, we demonstrate the system's capability to increase the AI index due to aging. Also, we consider a patient's waveform having high AI index, where the reconstructed waveform closely matches (Figure 6). One potential extension of our study involves the automatic determination of parameters in the 6-DOF model through a supervised machine learning algorithm. By incorporating this machine learning algorithm, our CAM-system can automatically generate desired waveforms by adjusting weights and delay parameters in each CAM when provided with the target waveforms. Recently, wearable devices in the form of wristbands and watches have attracted much attention in the digital health market to predict the risk of cardiovascular disease in daily life [36]. Standards for evaluating these devices have been proposed; therefore, a high-performance simulator is needed to accurately evaluate them [37]. Our system has yet to investigate the physiological significance of the modulation parameters we have developed to extend normal pulses to abnormal or disease pulses. In future research, our system will be used to accurately simulate essential predictive indices, such as vascular stiffness, continuous blood pressure, and irregular pulse rhythm. Furthermore, we aim for our system to evolve into a more versatile device capable of reproducing pulses indicative of certain medical conditions or various human disease. It will have the capability to generate pulses beyond the radial artery, including, the carotid artery, abdominal aorta, and coronary artery.

## REFERENCES

[1] M. Forouzanfar, H. R. Dajani, V. Z. Groza, M. Bolic, S. Rajan, and I. Batkin, "Ratio-independent blood pressure estimation by modeling the oscillometric waveform envelope," *IEEE Trans. Instrum. Meas.*, vol. 63, no. 10, pp. 2501–2503, Oct. 2014.

[2] K. Pesti, M. Metshein, P. Annus, H. Kõiv, and M. Min, "Electrode placement strategies for the measurement of radial artery bioimpedance: Simulations and experiments," *IEEE Trans. Instrum. Meas.*, vol. 70, pp. 1–10, 2021, Art. no. 9500610.

[3] M.-H. Jun and Y.-M. Kim, "Accuracy evaluation of robotic tonometry pulse sensor system based on radial artery pulse wave simulator," *IEEE Trans. Instrum. Meas.*, vol. 69, no. 10, pp. 7646–7657, Oct. 2020.

[4] D. Barvik, M. Cerny, and N. Noury, "The capacitive sensing of the pulsatile liquid flow—Investigation on a physical vascular model," *IEEE Trans. Instrum. Meas.*, vol. 72, pp. 1–8, 2023.

[5] K. R. Brinker and R. Zoughi, "Tunable chipless RFID pressure sensor utilizing additive manufacturing—Model, simulation, and measurement," *IEEE Trans. Instrum. Meas.*, vol. 72, pp. 1–6, 2023, Art. no. 8000813.

[6] C. Liu, D. Zheng, A. Murray, and C. Liu, "Modeling carotid and radial artery pulse pressure waveforms by curve fitting with Gaussian functions," *Biomed. Signal Process. Control*, vol. 8, no. 5, pp. 449–454, Sep. 2013.

[7] L. Wang, L. Xu, S. Feng, M. Q.-H. Meng, and K. Wang, "Multi-Gaussian fitting for pulse waveform using weighted least squares and multi-criteria decision making method," *Comput. Biol. Med.*, vol. 43, no. 11, pp. 1661–1672, Nov. 2013.

[8] L. Wang, L. Xu, D. Zhao, Y. Yao, and D. Song, "FPGA-based design and implementation of arterial pulse wave generator using piecewise Gaussian-cosine fitting," *Comput. Biol. Med.*, vol. 59, pp. 142–151, Apr. 2015.

[9] P. Comon, "Independent component analysis, a new concept?" *Signal Process.*, vol. 36, no. 3, pp. 287–314, Apr. 1994.

[10] A. Hyvärinen and E. Oja, "A fast fixed-point algorithm for independent component analysis," *Neural Comput.*, vol. 9, no. 7, pp. 1483–1492, Jul. 1997.

[11] Y.-H. Sun, T. J. Anderson, K. H. Parker, and J. V. Tyberg, "Wave-intensity analysis: A new approach to coronary hemodynamics," *J. Appl. Physiol.*, vol. 89, no. 4, pp. 1636–1644, Oct. 2000.

[12] C. J. H. Jones, M. Sugawara, Y. Kondoh, K. Uchida, and K. H. Parker, "Compression and expansion wavefront travel in canine ascending aortic flow: Wave intensity analysis," *Heart Vessels*, vol. 16, no. 3, pp. 91–98, Apr. 2002.

[13] K. H. Parker, "An introduction to wave intensity analysis," *Med. Biol. Eng. Comput.*, vol. 47, no. 2, pp. 175–188, Feb. 2009.

[14] M. Sugawara, K. Niki, N. Ohte, T. Okada, and A. Harada, "Clinical usefulness of wave intensity analysis," *Med. Biol. Eng. Comput.*, vol. 47, no. 2, pp. 197–206, Feb. 2009.

[15] S. Laxminarayan, P. Sipkema, and N. Westerhof, "Characterization of the arterial system in the time domain," *IEEE Trans. Biomed. Eng.*, vol. BME-2, no. 2, pp. 177–184, Mar. 1978.

[16] D. S. Berger, J. K. Li, W. K. Laskey, and A. Noordergraaf, "Repeated reflection of waves in the systemic arterial system," *Amer. J. Physiol.*, vol. 264, pp. H269–H281, Jan. 1993.

[17] D. S. Berger, J. K. Li, and A. Noordergraaf, "Differential effects of wave reflections and peripheral resistance on aortic blood pressure: A model-based study," *Amer. J. Physiol.-Heart Circulatory Physiol.*, vol. 266, no. 4, pp. H1626–H1642, Apr. 1994.

[18] B. E. Westerhof, I. Guelen, N. Westerhof, J. M. Karemaker, and A. Avolio, "Quantification of wave reflection in the human aorta from pressure alone: A proof of principle," *Hypertension*, vol. 48, no. 4, pp. 595–601, Oct. 2006.

[19] B. Hametner, S. Wassertheurer, J. Kropf, C. Mayer, A. Holzinger, B. Eber, and T. Weber, "Wave reflection quantification based on pressure waveforms alone—Methods, comparison, and clinical covariates," *Comput. Methods Programs Biomed.*, vol. 109, no. 3, pp. 250–259, Mar. 2013.

[20] G. Jo, T.-H. Yang, J. U. Kim, J.-H. Koo, and Y.-M. Kim, "Development of a mathematical model for age-dependent radial artery pulse wave analysis based on pulse waveform decomposition," *IEEE Access*, vol. 8, pp. 2963–2974, 2020.

[21] I. Doh, H. K. Lim, and B. Ahn, "Development of a simulator for the validation of noninvasive blood pressure-monitoring devices," *Blood Pressure Monitor.*, vol. 21, no. 3, pp. 189–191, Jun. 2016.

[22] *BP Pump 2 NIBP Blood Pressure Simulator*. Accessed: May 6, 2024. [Online]. Available: https://www.flukebiomedical.com/products/biomedical-test-equipment/patient-simulators/bp-pump-2-nibp-blood-pressure-simulator

[23] *Satellite Infuse/Withdraw PHD ULTRA? Syringe Pumps*. Accessed: May 6, 2024. [Online]. Available: https://www.harvardapparatus.com/satellite-infuse-withdraw-phd-ultra-153-syringe-pumps.html

[24] *Arterial Puncture Training Wrist*. Accessed: May 6, 2024. [Online]. Available: https://www.kyotokagaku.com/en/products_data/m99/

[25] *Cardiovascular Waveform Pump*. Accessed: May 6, 2024. [Online]. Available: https://www.harvardapparatus.com/catalog/product/view/id/8294/s/pulsatile-blood -pumps/category/78/

[26] *Endovascular Simulator Creates Physiological Pulsatile Flow and Pressures*. Accessed: May 6, 2024. [Online]. Available: https://vivitrolabs.com/product/endovascular-ev-simulator/

[27] D. Legendre, J. Fonseca, A. Andrade, J. F. Biscegli, R. Manrique, D. Guerrino, A. K. Prakasan, J. P. Ortiz, and J. C. Lucchi, "Mock circulatory system for the evaluation of left ventricular assist devices, endoluminal prostheses, and vascular diseases," *Artif. Organs*, vol. 32, no. 6, pp. 461–467, Jun. 2008.

[28] R. Zannoli, I. Corazza, and A. Branzi, "Mechanical simulator of the cardiovascular system," *Phys. Medica*, vol. 25, no. 2, pp. 94–100, Jun. 2009.

[29] Y. Yokoyama, O. Kawaguchi, T. Shinshi, U. Steinseifer, and S. Takatani, "A new pulse duplicator with a passive fill ventricle for analysis of cardiac dynamics," *J. Artif. Organs*, vol. 13, no. 4, pp. 189–196, Dec. 2010.

[30] J. Brum, D. Bia, N. Benech, G. Balay, R. Armentano, and C. Negreira, "Set up of a cardiovascular simulator: Application to the evaluation of the dynamical behavior of atheroma plaques in human arteries," *Phys. Procedia*, vol. 3, no. 1, pp. 1095–1101, Jan. 2010.

[31] L. A. Foley, "Development of a cardiovascular simulator incorporating a phantom simulation of the arterial system," Ph.D. dissertation, School Eng., Auckland Univ. Technol., Auckland, New Zealand, 2021.

[32] E. S. Rapp, S. R. Pawar, and R. G. Longoria, "Hybrid mock circulatory loop simulation of extreme cardiac events," *IEEE Trans. Biomed. Eng.*, vol. 69, no. 9, pp. 2883–2892, Sep. 2022.
[33] D.-J. Kim, G. Jo, J.-H. Koo, T.-H. Yang, and Y.-M. Kim, "Development of a simulator capable of generating age-specific pulse pressure waveforms for medical palpation training," *Appl. Sci.*, vol. 12, no. 22, p. 11555, Nov. 2022.
[34] T.-H. Yang, G. Jo, J.-H. Koo, S.-Y. Woo, J. U. Kim, and Y.-M. Kim, "A compact pulsatile simulator based on cam-follower mechanism for generating radial pulse waveforms," *Biomed. Eng. OnLine*, vol. 18, no. 1, pp. 1–18, Dec. 2019.
[35] P. R. Fleming, "The mechanism of the pulsus bisferiens," *Heart*, vol. 19, no. 4, pp. 519–524, Oct. 1957, doi: 10.1136/hrt.19.4.519.
[36] K. Bayoumy, M. Gaber, A. Elshafeey, O. Mhaimeed, E. H. Dineen, F. A. Marvel, S. S. Martin, E. D. Muse, M. P. Turakhia, K. G. Tarakji, and M. B. Elshazly, "Smart wearable devices in cardiovascular care: Where we are and how to move forward," *Nature Rev. Cardiol.*, vol. 18, no. 8, pp. 581–599, Aug. 2021.
[37] *Traditional Chinese Medicine-General Requirements of Electric Radial Pulse Tonometric Devices*, ISO Standard 18615, 2020.

**TAE-HEON YANG** received the B.S. degree from Yonsei University, Seoul, in 2006, and the M.S. and Ph.D. degrees from the Department of Mechanical Engineering, Korea Advanced Institute of Science and Technology (KAIST), in 2008 and 2012, respectively. From 2012 to 2017, he was a Senior Research Scientist with Korea Research Institute of Standards and Science. From 2018 to 2023, he was with the Faculty of Electronic Engineering, Korea National University. He is currently an Associate Professor of mechanical engineering with Konkuk University, Seoul.

**JAE-IK KIM** received the B.S. degree in control and instrumentation engineering and the M.S. degree in electronic engineering from Korea National University of Transportation, in 2020 and 2022, respectively, where he is currently pursuing the Ph.D. degree. His research interests include haptic sensors and actuators.

**JEONG-HOI KOO** received the Ph.D. degree in mechanical engineering from Virginia Tech, in 2003. He is currently a Professor of mechanical and manufacturing engineering with Miami University, Oxford, OH, USA. His research interests include smart materials and systems and humanitarian engineering. He was elected as a fellow of the American Society of Mechanical Engineers (ASME), in 2019. He is also serving as an Associate Editor for the *Journal of Vibration and Control*, *Shock and Vibration* journal, and *Frontiers in Materials–Smart Materials*.

**GWANGHYUN JO** received the B.S., M.S., and Ph.D. degrees from the Department of Mathematical Sciences, Korea Advanced Institute of Science and Technology (KAIST), Daejeon, South Korea, in 2018. From 2018 to August 2019, he was a Postdoctoral Researcher with KAIST. Since 2023, he has been a Faculty Member with the Department of Mathematical Data Science, Hanyang University, ERICA Campus. His research interests include numerical analysis and simulation of various fluids problems arising from hemodynamics, and petroleum engineering.

**YOUNG-MIN KIM** received the B.S. degree in mechanical engineering from Yonsei University, Seoul Korea, in 1999, the M.S. degree in mechanical engineering from POSTECH, South Korea, in 2001, and the Ph.D. degree in mechanical engineering from Korea Advanced Institute of Science and Technology (KAIST), South Korea, in 2011. From 2022 to 2026, he was a Research Scientist with the Human-Welfare Robotic System Center, KAIST. Since 2011, he has been a Principal Researcher with the Digital Health Research Division, Korea Institute of Oriental Medicine, South Korea. His research interests include the medical devices for personalized healthcare, wearable sensors for daily health monitoring, sophisticated human-robot interface (HRI) technology, and innovative HRI applications.